Original Article
Decoding the pro-invasive role of SAA2 in renal cell carcinoma: an exploratory study and experimental validation

Yin Chen[*], Haoqing Shi[*], Yifan Xu, Zhiyuan Zhuo

Department of Urology, Changhai Hospital, Naval Medical University, Shanghai, China. [*]Equal contributors.

Abstract: Purpose: Currently, there is an urgent need for prognostic prediction models for renal clear cell carcinoma (ccRCC). This study aims to establish a prognostic prediction model based on differential genes associated with TNM staging and validate it through both in vitro and in vivo experiments. Method: Through the cross-analysis of the differential genes between T1-2 and T3-4 stages, N1 and N2 stages, as well as M0 and M1 stages in ccRCC, a nomogram prognostic model was constructed using multivariate COX regression analysis. Finally, the function of human serum amyloid A2 (SAA2) was verified through in vivo and in vitro experiments. Result: Through cross-analysis of the differential genes between T1-2 and T3-4 stages, N1 and N2 stages, as well as M0 and M1 stages, 67 genes were identified. Through multivariate COX regression analysis, examination of expression differences between cancerous and normal tissues, and assessment of their impact on prognosis, we have derived a nomogram prognostic prediction model composed of ITPKA, PDIA2, SAA2, SHOX2, TREML3P, and ZIC2. Furthermore, through Transwell migration and invasion assays, EdU proliferation assays, and in vivo experiments, we validated that SAA2 promotes the proliferation, migration, and invasion of ccRCC. Conclusion: The nomogram prognostic prediction model, consisting of ITPKA, PDIA2, SAA2, SHOX2, TREML3P, and ZIC2, is capable of predicting the prognosis of ccRCC patients. Among them, SAA2 promotes the proliferation, migration, and invasion of ccRCC cells.

Keywords: Clear cell renal cell carcinoma, TNM, nomogram, serum amyloid A2

Introduction

Renal cell carcinoma (RCC) represents one of the most prevalent malignancies in the urinary system, with its global incidence demonstrating a persistent annual increase of approximately 2% over the past two decades, posing substantial challenges to public health worldwide [1, 2]. Among all RCC subtypes, clear cell renal cell carcinoma (ccRCC) constitutes the predominant histological variant, accounting for 70-80% of cases [3]. Clinically, the insidious nature of early-stage ccRCC-characterized by nonspecific symptoms - frequently leads to delayed diagnosis, with approximately 40% of patients presenting with advanced or metastatic disease at initial diagnosis [4, 5]. Notably, even among patients undergoing radical nephrectomy for localized ccRCC, approximately 25% develop locoregional recurrence or distant metastasis, correlating with a marked decline in 5-year survival rates [6-8]. Current therapeutic strategies for metastatic ccRCC remain limited, yielding a median overall survival of merely 12 months despite multimodal interventions [9]. These sobering statistics underscore the critical need to elucidate the molecular drivers of ccRCC pathogenesis and identify novel therapeutic targets and prognostic biomarkers to improve clinical outcomes. The identification of genes and proteins critically involved in tumorigenesis and progression remains a central focus in oncology research.

Accumulating evidence indicates that numerous inflammation-associated proteins exhibit dysregulated expression within tumor microenvironments, driving oncogenesis through modulation of cellular proliferation, migration, invasion, and immune evasion mechanisms [10-12]. In this study, we performed cross-analysis of differentially expressed genes (DEGs) be-

tween T1-2 vs T3-4 stages, N0 vs N1 stages, and M0 vs M1 stages, identifying a 6-gene signature that formed the basis for constructing a prognostic nomogram model. Among these candidates, serum amyloid A2 (SAA2) - an acute-phase reactant implicated in inflammatory pathologies and various malignancies - was selected for experimental validation [13, 14]. While emerging data suggest SAA2 expression correlates with tumor grade and survival outcomes in RCC [15], its precise mechanistic contributions to ccRCC pathogenesis remain incompletely characterized. Furthermore, current diagnostic and prognostic models for ccRCC predominantly rely on clinicopathological parameters and conventional biomarkers, with limited integration of molecular pathogenesis insights, thereby constraining their predictive accuracy and clinical utility.

This investigation aims to: (1) systematically delineate the functional role and molecular mechanisms of SAA2 in ccRCC progression, and (2) develop a novel prognostic model integrating molecular signatures with clinical variables to enhance therapeutic decision-making. Our integrative approach bridges molecular oncology with clinical prediction modeling, offering both mechanistic insights into SAA2-driven oncogenesis and a precision medicine tool for ccRCC management.

Methods

Bioinformatics analysis

Datasets: For this study, we acquired a training dataset from the TCGA-KIRC database, a part of The Cancer Genome Atlas (TCGA). This dataset consisted of gene expression profiles obtained from 537 tumor tissues and 72 samples of normal tissue, along with accompanying clinical information. To maintain data integrity, we excluded genes with raw counts below 10 in over 25% of the samples.

Difference analysis: Using the "DESeq2" package, differential expression analysis was performed on cancer versus paracancerous tissues from T1-2 versus T3-4 stages, N0 versus N1 stages, and M0 versus M1 stages [*p* value <0.01, |log2fold change (FC)|>1] to identify differentially expressed genes (DEGs). Following this, the intersection genes were integrated with the DEGs, and the overlapping set was

determined to obtain target genes (TGs). Gene Ontology (GO) and Kyoto Encyclopedia of Genes and Genomes (KEGG) analyses of the TGs were conducted using the "clusterProfiler" package.

Construction of nomogram model: Through univariate and multivariate COX regression analyses of the TGs obtained from the aforementioned differential analysis, genes associated with overall survival (OS) were identified based on a significance threshold of P < 0.05 to construct a nomogram model, and a risk coefficient was determined for each gene. Subsequently, the expression level of each selected gene was multiplied by its corresponding risk coefficient to calculate the risk score for each patient. Patients were then stratified into different risk groups based on the median risk score. To evaluate the discriminative ability of the model across various risk levels, Kaplan-Meier survival analyses were performed.

In vivo and in vitro experimental validation

Cell lines and cell culture: The RCC cell lines (786-O, A498) were obtained from the Cell Bank of the Chinese Academy of Sciences. The cells were cultured in a constant temperature incubator at 37°C with 5% CO_2. The growth medium for 786-O cells consisted of RPMI-1640 (S11875500BT, Gibco Life Technologies, America), while MEM (C12571500BT, Gibco Life Technologies, America) was used for A498 cells, both supplemented with 10% fetal bovine serum (FBS, 164210, Pricella Biotechnology Co., Ltd., Hubei, China) and 1% antibiotics. No mycoplasma contamination was detected, and the authenticity of 786-O and A498 was verified using the short tandem repeat (STR) method.

Western blot (WB): Upon reaching confluence, cellular proteins are extracted using pre-cooled RIPA lysis buffer (P0013B, Beyotime Biotech Co. Ltd., Shanghai, China) containing 1% PMSF (ST505, Beyotime Biotech Co. Ltd., Shanghai, China). The cells are then lysed on ice for 30 minutes, followed by sonication and shaking. Subsequently, the supernatant is obtained by centrifugation (Eppendorf, 5804R, German) at 4°C and 12,000 rpm for 10 minutes. The protein concentration is determined using the BCA (P0009, Beyotime Biotech Co. Ltd., Shanghai, China) method. After adjusting the sample concentration, 25% volume of 5× loading buffer

(P0286, Beyotime Biotech Co. Ltd., Shanghai, China) is added and thoroughly mixed. Denaturation is achieved in a metal bath at 99°C for 10 minutes. Then, gels are prepared for protein separation, followed by the electrophoretic transfer of the proteins onto NC membranes (HATF00010, Merck Millipore Ltd., America). Subsequently, the membranes are incubated with designated primary antibodies (beta-Tubulin, 10068-1-AP, proteintech Biotech Co. Ltd., Hubei, China. SAA2, YB70765, Yubo Biotech Co. Ltd., Shanghai, China) at a dilution ratio of 1:1000 overnight at 4°C, followed by incubation with corresponding secondary antibodies (SA00001-1/2, proteintech Biotech Co. Ltd., Hubei, China) at a dilution ratio of 1:1000 for 1 hour at room temperature.

In vivo and in vitro functional validation: We performed overexpression and knockdown of SAA2 in ccRCC lines 786-O and A498 using overexpression plasmids (overexpression plasmid sequence: atgaagcttctcacgggcctggttttct-gctccttggtcctgagtgtcagcagccgaagcttcttttc-gttccttggcgaggcttttgatggggctcgggacatgtg-gagagcctactctgacatgagagaagccaattacatcggct-cagacaaatacttccatgctcggggggaactatgatgctgc-caaaaggggacctgggggtgcctgggctgcagaagtgat-cagcaatgccagagagaatatccagagactcacaggcc-gtggtgcggaggactcgctggccgatcaggctgccaata-aatggggcaggagtggcagagaccccaatcacttcc-gacctgctggcctgcctgagaaatactga) and short hairpin RNA (shRNA sequence: CATGAGAGAAG-CCAATTACAT). The protein expression level of SAA2 after transfection was assessed via WB to verify the accuracy and effectiveness of the transfection. Subsequently, we conducted a series of in vitro experiments to assess the impact of SAA2.

We conducted an EdU proliferation assay (C10310, RiboBio, Co. Ltd., Guangdong, China) to evaluate the cell proliferation capacity. 786-O and A498 cells were seeded in 6-well plates, and when the cell density reached 60%-70%, EdU reagent was added and incubated for 2 hours. Subsequently, the cells were fixed with 4% paraformaldehyde for 30 minutes, and then 2 mg/ml glycine solution was added to each well. The cells were permeabilized with Triton X-100 (P0096, Beyotime Biotech Co. Ltd., Shanghai, China) for 10 minutes, and then 1 ml of Apollo staining reaction solution was added to each well and incubated for 30 minutes. Finally, the cells were stained with DAPI (C1002,

Beyotime Biotech Co. Ltd., Shanghai, China) for 5 minutes and observed under a fluorescence microscope.

The migration and invasion capabilities of ccRCC cells were evaluated through Transwell migration and invasion assays (3422, Corning Ltd., America). Cells were seeded in 24-well Transwell chambers that were pre-coated with or without Matrigel matrix gel (356234, Corning Ltd., America). Approximately 20,000 cells were added to each upper chamber in a medium without FBS, while the lower chamber contained a medium with 10% FBS. After 24 hours, the cells were fixed, stained, and counted.

To further validate the function of SAA2 in vivo, we conducted a subcutaneous tumor-bearing experiment using nude mice. We obtained 10 BALB/c nude mice (4-week-old, male, from jh-labanimal, China) and injected SAA2-overexpressing 786O cells and control cells into the subcutaneous tissue of the mice. After 14 days, the nude mice were euthanized and dissected, and the tumor growth and weight were observed and compared. Tumor dimensions were measured every 3 days, with the longest diameter (L) and shortest diameter (W) recorded. Tumor volume was calculated using the formula: $V = L{\times}W^2/2$. In this study, mice were anesthetized using tribromoethanol (Avertin, Merck, T48402) and were humanely euthanized by cervical dislocation at the end of the experimental procedures. All animal experiments were conducted in compliance with relevant regulations, policies, and guidelines. All animal experiments in this study were conducted at the SPF-grade Animal Research Center of Naval Medical University. The experimental protocols were approved by the Institutional Animal Care and Use Committee of Naval Medical University [Approval No. CHEC (A.E)2024-011].

Statistical analysis

Statistical analyses were conducted using R (version 4.2.2) or GraphPad Prism (version 9.0), with a statistical significance level set at $P < 0.05$. Categorical variables were compared using chi-square test, while t-tests were utilized for comparing continuous variables. Statistical analysis was performed using one-way ANOVA to compare results among the three groups, followed by appropriate post hoc tests (Tukey's HSD) for pairwise comparisons between the

experimental groups. The correlations among continuous variables were assessed through Spearman or Pearson correlation analysis.

Results

Screening and preliminary analysis of target genes

We conducted a cross-analysis of the DEGs between T1-2 and T3-4 stages, N0 and N1 stages, as well as M0 and M1 stages in the TCGA-KIRC dataset. The Venn diagram revealed that these three sets of DEGs shared 67 target genes in total (**Figure 1A**). Subsequently, we performed both univariate and multivariate COX regression analyses on these 67 genes. The forest plot showed that only eight genes, namely ZIC2 [Hazard ratio (HR) = 1.840, 95% Confidence interval (CI) = 1.256-2.695], OTX1 (HR = 1.466, 95% CI = 1.029-2.090), SAA2 (HR = 1.650, 95% CI = 1.056-2.579), ITPKA (HR = 1.629, 95% CI = 1.088-2.438), GPR78 (HR = 1.892, 95% CI = 1.312-2.730), SHOX2 (HR = 1.758, 95% CI = 1.216-2.540), TREML3P (HR = 1.431, 95% CI = 1.030-1.987), and PDIA2 (HR = 1.458, 95% CI = 1.023-2.077), were statistically significant (P < 0.05) (**Figure 1B**). Next, we conducted a preliminary screening of the expression levels of these eight genes between paired ccRCC tissues and normal kidney tissues. As shown in **Figure 1C**, there were significant differences in the expression levels of ZIC2, SAA2, ITPKA, SHOX2, TREML3P, and PDIA2 between ccRCC tumor tissues and normal kidney tissues, with higher expression levels observed in tumor tissues. However, no significant difference was found in the expression levels of OTX1 and GPR78 between ccRCC tumor tissues and normal kidney tissues. Next, we further analyzed the effects of the expression levels of ZIC2, SAA2, ITPKA, SHOX2, TREML3P, and PDIA2 in ccRCC tissues on the survival time of patients. Not surprisingly, the high expression of ZIC2, SAA2, ITPKA, SHOX2, TREML3P, and PDIA2 in tumor tissues can all lead to worse prognosis for patients (**Figure 1D**). Therefore, we will further analyze the six genes, ZIC2, SAA2, ITPKA, SHOX2, TREML3P, and PDIA2, as target genes next.

Subsequently, we conducted clinical relevance analysis on ZIC2, SAA2, ITPKA, SHOX2, TREML3P, and PDIA2. For pathological T stage, N stage and M stage, we found that high expressions of ZIC2, SAA2, ITPKA, SHOX2, TREML3P,

and PDIA2 in tumor tissues corresponded to higher T stage, N stage and M stage (**Figure 2A-C**). Similiarly, we investigated the impact of ZIC2, SAA2, ITPKA, SHOX2, TREML3P, and PDIA2 on pathological grading and obtained the same results (**Figure 2D**).

Construction of nomogram model

Based on the above analysis results, we further combined ZIC2, SAA2, ITPKA, SHOX2, TREML3P, and PDIA2 as a gene panel to construct a nomogram risk prediction model (**Figure 3A**), and indicated the predictive values of this model for 1-year, 3-year, and 5-year survival probabilities.

Using the nomogram model, we assigned scores to and grouped the patients in TCGA-KIRC, dividing them into a high-risk group and a low-risk group based on the median (Riskscore = -0.1831) as the boundary. The risk-factor chart revealed that the expression levels of the six genes in the high-risk group were significantly higher than those in the low-risk group, and the number of patient deaths was also significantly higher in the high-risk group. Additionally, as the Riskscore increased, the number of deaths further increased (**Figure 3B**). Through Kaplan-Meier survival curve analysis, we found that the high-risk group indeed had a worse survival period (HR = 2.84, 95% CI = 2.06-3.93) (**Figure 3C**). Through literature search, we found that the functions of ZIC2, ITPKA, SHOX2, TREML3P, and PDIA2 have been verified in previous studies, while SAA2 has not been verified and explored by researchers yet. Therefore, we chose SAA2 for further experimental verification. The predictive performance of the nomogram was rigorously evaluated using ROC analysis (**Figure 3D**). The model demonstrated an AUC of 0.757 (95% CI: 0.713-0.801), compared to the T-stage-based model, which yielded a significantly lower AUC of 0.677 (95% CI: 0.630-0.723) (P < 0.001). These results confirm the statistically significant improvement in prognostic stratification achieved by our nomogram model, highlighting its superior predictive accuracy for RCC progression.

SAA2 can promote the proliferation, migration, and invasion capabilities of ccRCC cells

We overexpressed SAA2 in 786O and A498 cells respectively, and confirmed this overexpression through Western Blotting (WB) (**Figure 4E**). Subsequently, we used Transwell migra-
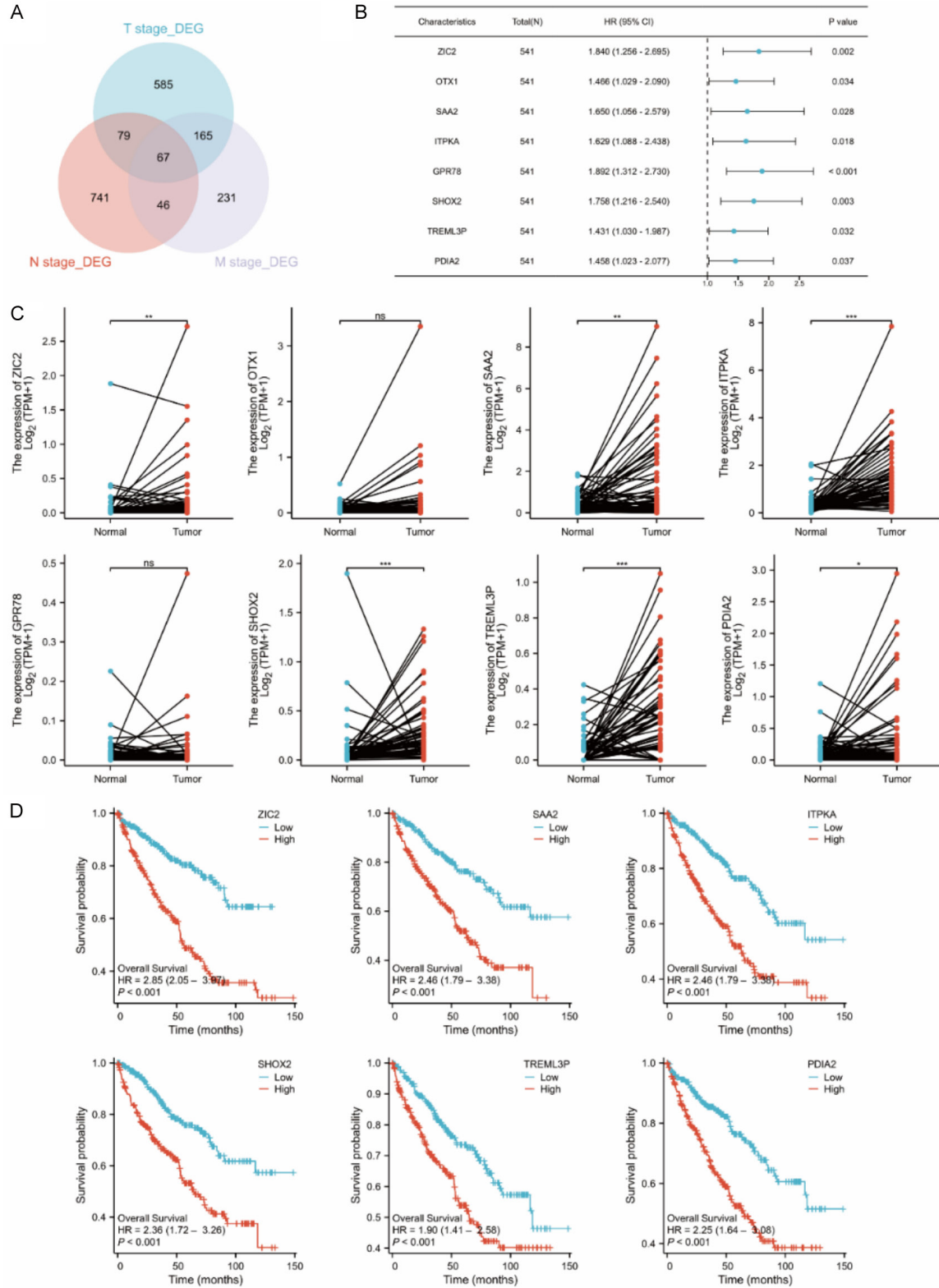
Figure 1. Identification of key genes driving ccRCC progression through differential gene expression analysis across TNM stages. A. Venn plot shows cross analysis of differential genes between T1-2 and T3-4 phases, N0 and N1 phases, and M0 and M1 phases of ccRCC. B. Forest plot of multi factor COX regression analysis. C. Expression levels of ZIC2, OTX1, SAA2, ITPKA, GPR78, SHOX2, TREML3P, PDIA2 in ccRCC tumor tissue and normal tissue. D. Kaplan Meier survival analysis of ZIC2, SAA2, ITPKA, SHOX2, TREML3P, PDIA2 in predicting the prognosis of ccRCC patients.
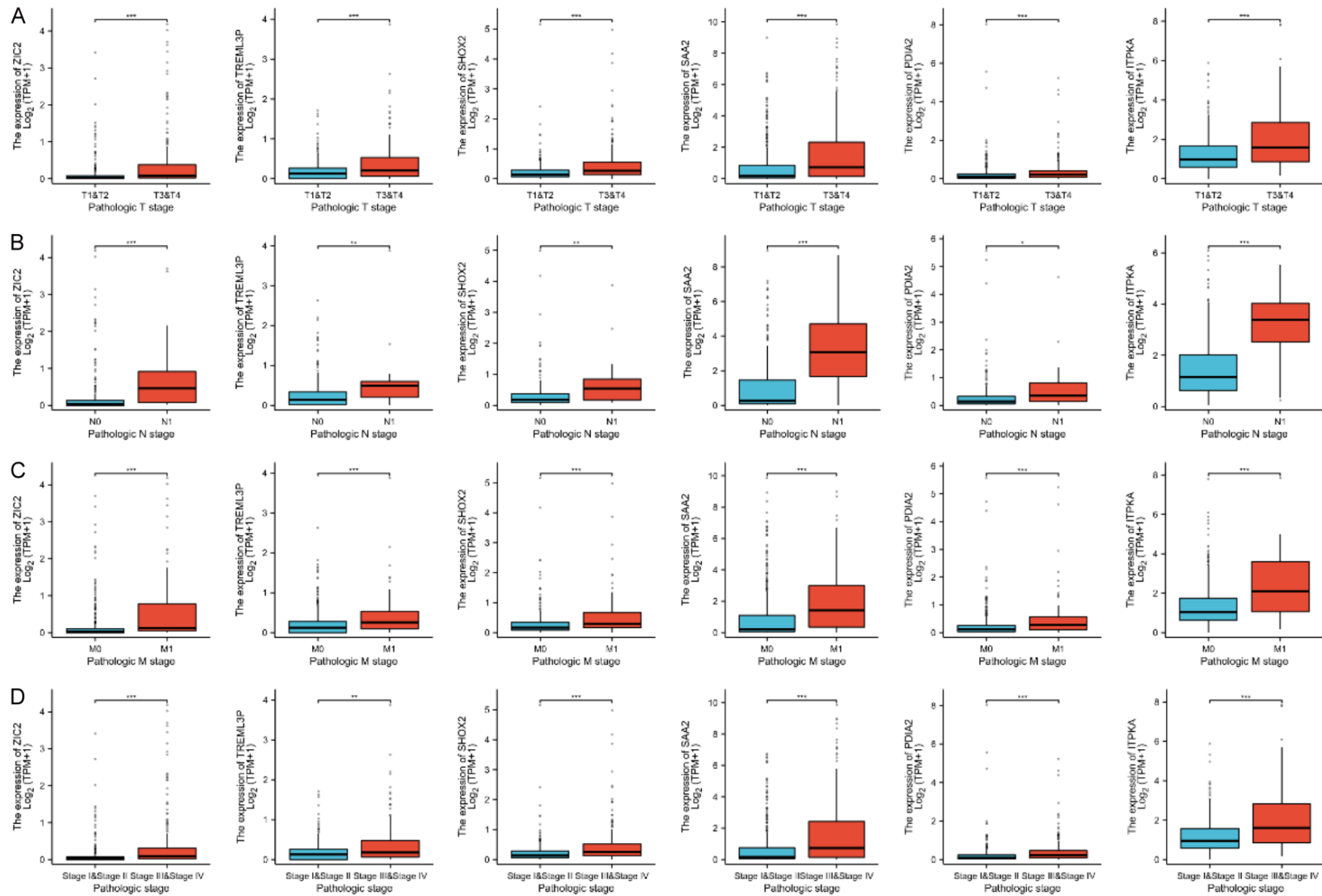
Figure 2. Differential expression patterns of key genes and their clinicopathological correlations. A. Differential expression of ZIC2, SAA2, ITPKA, SHOX2, TREML3P, PDIA2 in ccRCC during T1-2 and T3-4 phases. B. Differential expression of ZIC2, SAA2, ITPKA, SHOX2, TREML3P, PDIA2 in ccRCC of N0 and N1 stages. C. Differential expression of ZIC2, SAA2, ITPKA, SHOX2, TREML3P, PDIA2 in M0 and M1 ccRCC. D. Differential expression of ZIC2, SAA2, ITPKA, SHOX2, TREML3P, PDIA2 in WHO/ISUP I-II and III-IV grade ccRCC.
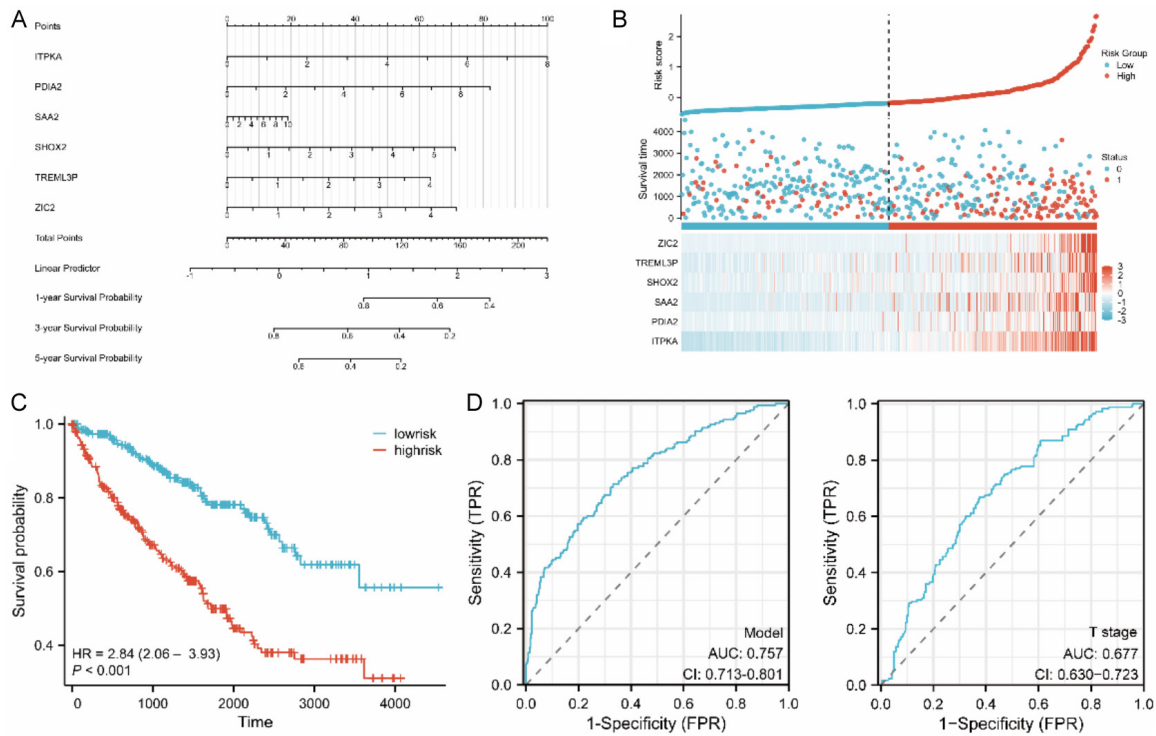
Figure 3. Development of a key gene-based nomogram model for predicting ccRCC prognosis. A. Nomogram prognostic prediction model constructed by ZIC2, SAA2, ITPKA, SHOX2, TREML3P, PDIA2. B. Risk factor map of nomogram prognostic prediction model constructed by ZIC2, SAA2, ITPKA, SHOX2, TREML3P, PDIA2. C. Kaplan Meier survival analysis of high-risk and low-risk groups divided by nomogram prognostic prediction model. D. Comparison of ROC curve between the nomogram and T stage.

tion assays and Transwell invasion assays to verify the migration and invasion capabilities of the SAA2-overexpressed 7860 and A498 cell lines, respectively. The results showed that the 7860 and A498 cell lines overexpressing SAA2 exhibited stronger migration and invasion abilities (**Figure 4A**, **4B**). In addition, we also performed EdU proliferation assays to verify that the 7860 and A498 cell lines overexpressing SAA2 had enhanced proliferation capabilities (**Figure 4C**, **4D**).

We knocked down SAA2 in 7860 and A498 cells respectively, and confirmed this knockdown through Western Blotting (WB) (**Figure 4F**). Subsequently, we used Transwell migration assays and Transwell invasion assays to verify the migration and invasion capabilities of the SAA2-knockdown 7860 and A498 cell lines, respectively. The results showed that the 7860 and A498 cell lines with SAA2 knockdown exhibited weaker migration and invasion abilities (**Figure 5A**, **5B**). In addition, we also performed EdU proliferation assays to verify that the 7860 and A498 cell lines with SAA2 knock-

down had reduced proliferation capabilities (**Figure 5C**, **5D**).

Finally, we conducted in vivo validation experiments to investigate the proliferation capacity of SAA2-overexpressing ccRCC cell lines in vivo. We implanted the ccRCC cell lines subcutaneously into the axillary region of BALB/c nude mice. After two weeks, the mice were euthanized, and the tumors were dissected. The results showed that the ccRCC cells overexpressing SAA2 had stronger in vivo proliferation capacity, with larger tumor weights and volumes compared to the control group (**Figure 6A**, **6B**).

Analysis of the downstream mechanisms of SAA2

To further investigate how SAA2 affects downstream molecules in ccRCC cells, we conducted a differential analysis of samples with high and low SAA2 expression in TCGA-KIRC, identifying 311 upregulated genes and 178 downregulated genes (**Figure 7A**). The heatmap
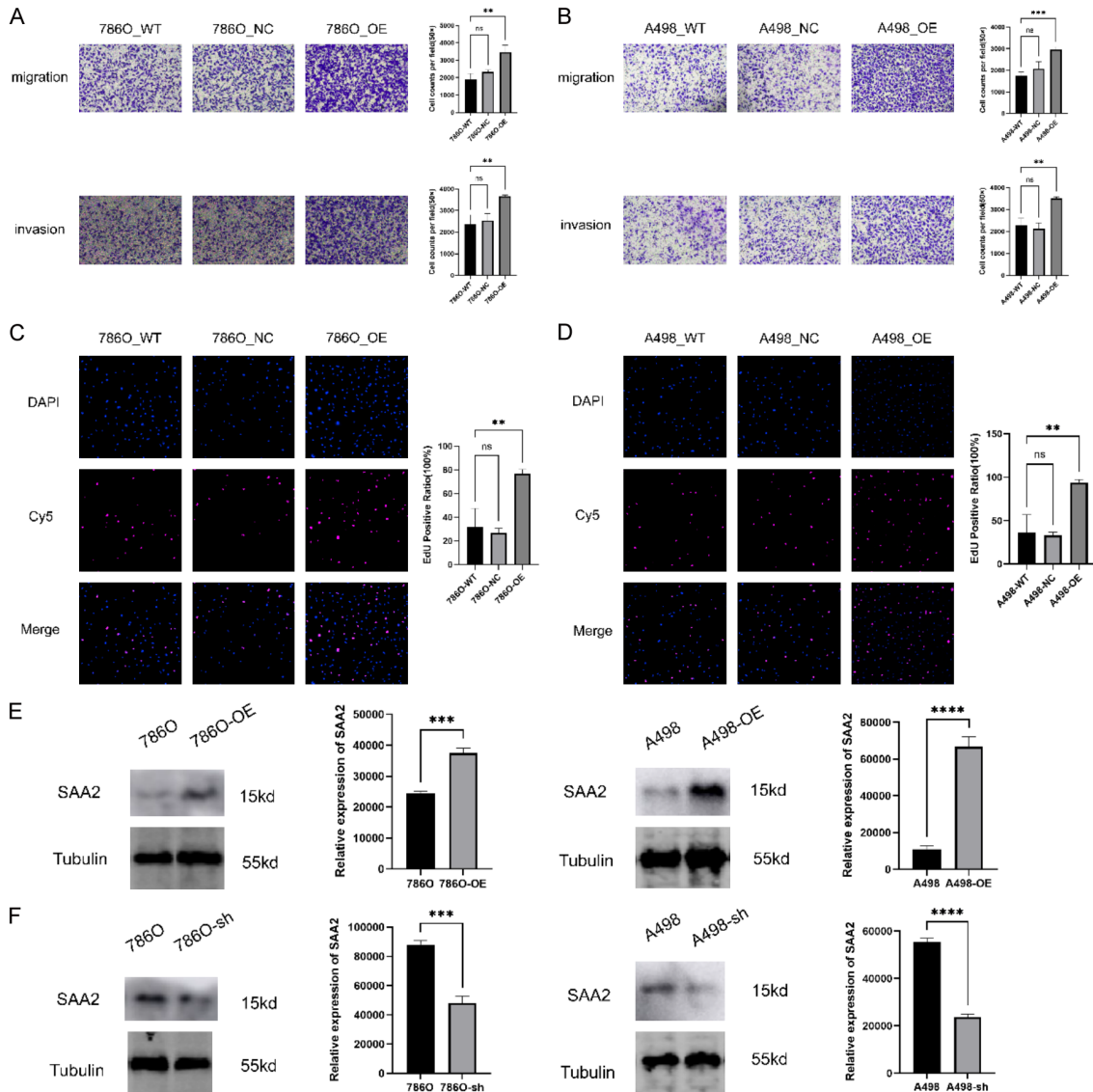
Figure 4. SAA2 overexpression promotes proliferation and migration in ccRCC. A. Transwell migration and invasion assays of 786O cells overexpressing SAA2. B. Transwell migration and invasion assays of A498 cells overexpressing SAA2. C. EdU proliferation assays of 786O overexpressing SAA2. D. EdU proliferation assays of A498 overexpressing SAA2. E. Western blotting of 786O and A498 overexpression of SAA2. F. Western blotting of 786O and A498 knockdown of SAA2.

shows that MYL3, PTH1R, SLC6A19, C1orf210, FRMD3, TRPM3, ALDH6A1, TMEM38B, MAP7, and CLCN5 are the top ten highly expressed genes in the high-risk group, while KCNG1, ADAMTS14, COL22A1, PDGFRL, MOCOS, SAA1, ITPKA, LINC00460, STEAP3, and GFPT2 are the top ten genes with high expression in the low-risk group (**Figure 7B**). Subsequently, we performed GO and KEGG pathway analyses on the differentially expressed genes downstream of SAA2 (**Figure 7C**) and presented each molecule's corresponding GO and KEGG pathways in

a chord diagram (**Figure 7D**). We found that the upregulated molecules downstream of SAA2 are primarily concentrated in extracellular matrix-related pathways, suggesting that SAA2 likely influences tumor microenvironment and subsequent tumor development by modulating the extracellular matrix of tumor cells.

Discussion

SAA2 is a tissue-specific protein that possesses various crucial molecular functions within
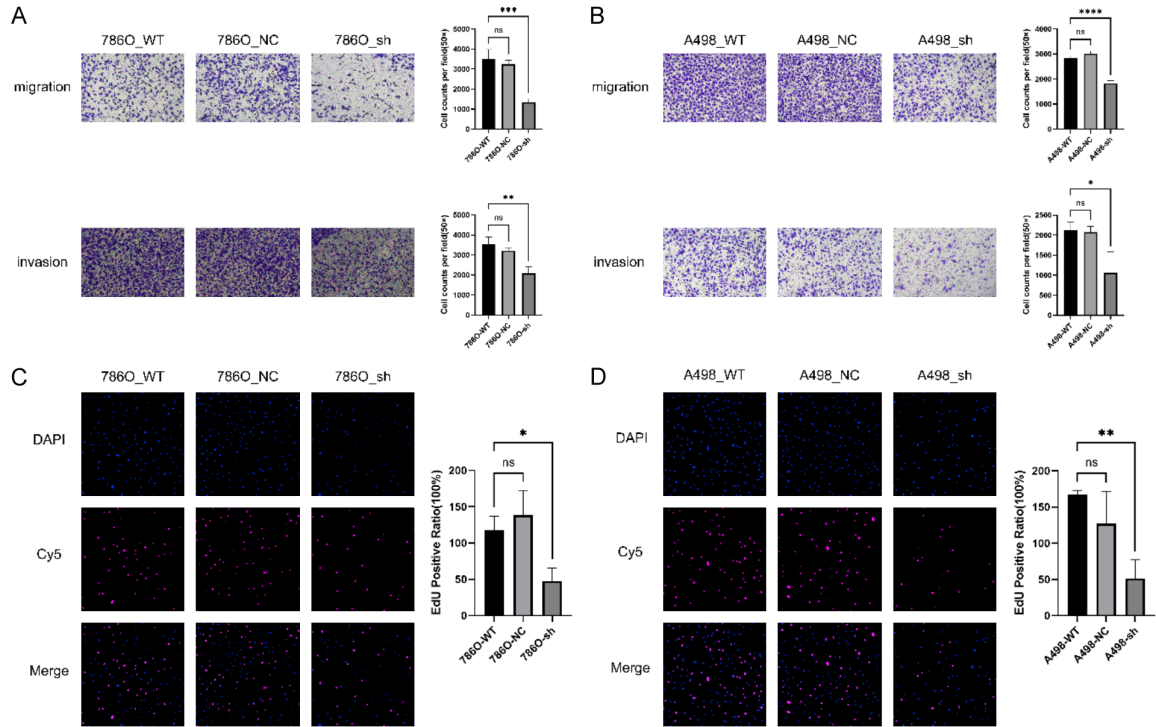
Figure 5. SAA2 knockdown suppresses proliferation and migration in ccRCC. A. Transwell migration and invasion assays of knocking down SAA2 in 786O. B. Transwell migration and invasion assays of knocking down SAA2 in A498. C. EdU proliferation experiment of knocking down SAA2 in 786O. D. EdU proliferation experiment of knocking down SAA2 in A498.
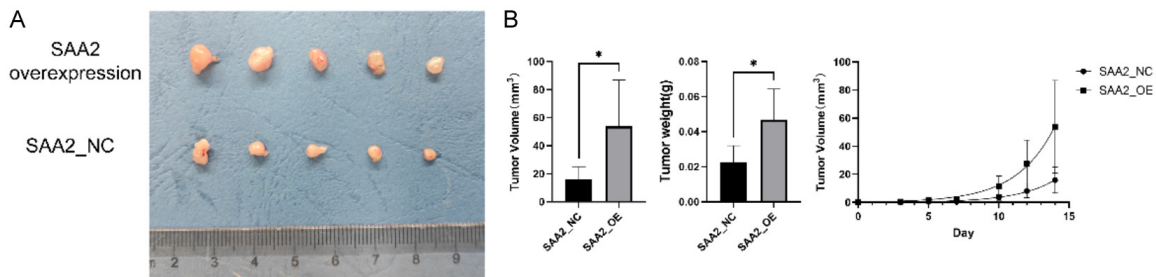
Figure 6. In vivo experiments validate that SAA2 overexpression promotes ccRCC invasion. A. Subcutaneous tumors overexpressing SAA2 in 786O and control group 786O. B. The bar chart displays the tumor volume and weight of the SAA2 overexpression group and the control group, as well as the tumor volume growth curve from 0-15 days.

the body [16-18]. It plays a pivotal role in the immune system by modulating immune responses [19, 20]. By interacting with other proteins, SAA2 participates in the activation and signaling of immune cells, thereby regulating the functionality of the immune system [21, 22]. Furthermore, SAA2 can bind to cell surface receptors, mediating signaling pathways that accelerate cell proliferation [23]. This is essential for tissue repair and regeneration processes. Through its interaction with cell surface

receptors, SAA2 triggers a cascade of signaling transduction events, ultimately influencing the physiological functions and behaviors of cells [24].

Through systematic integration of in vitro cellular experiments and in vivo animal modeling, this study mechanistically delineates the functional role of SAA2 in RCC progression. Our findings demonstrate that SAA2 is consistently upregulated in RCC cell lines, with its expres-
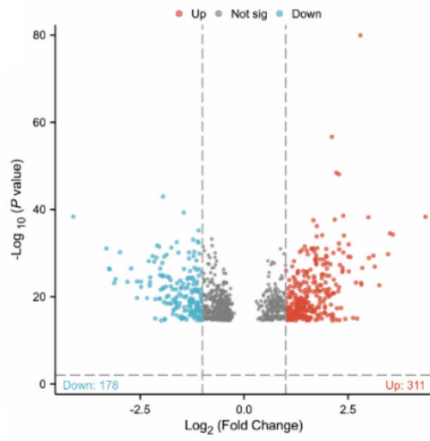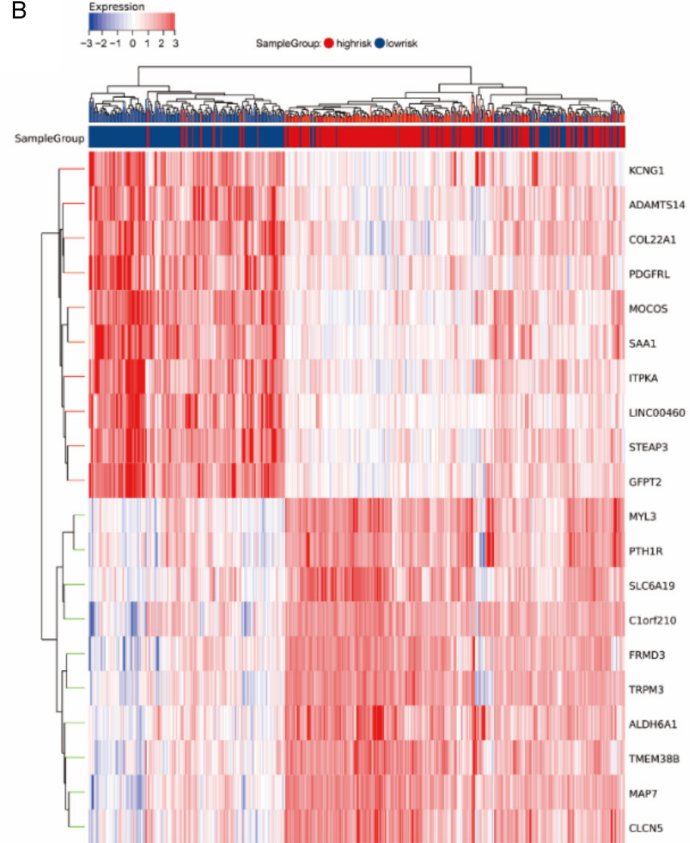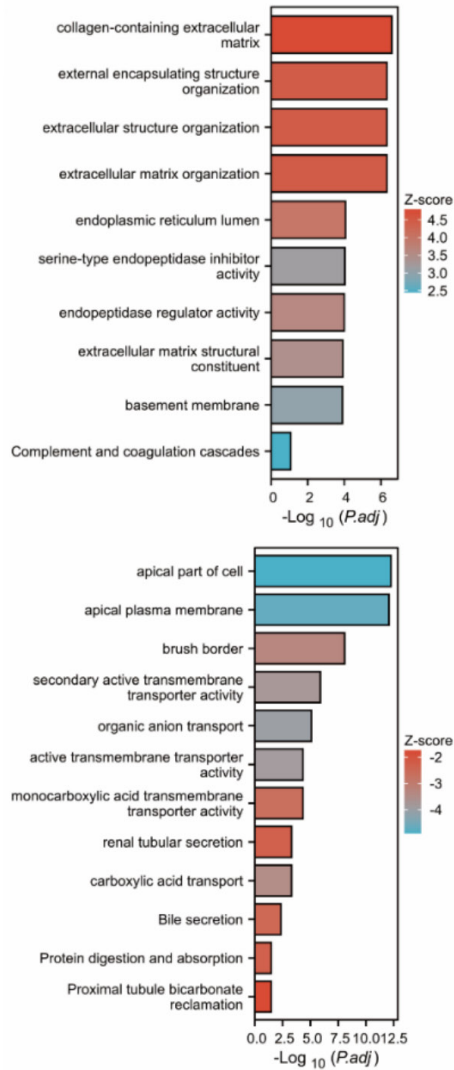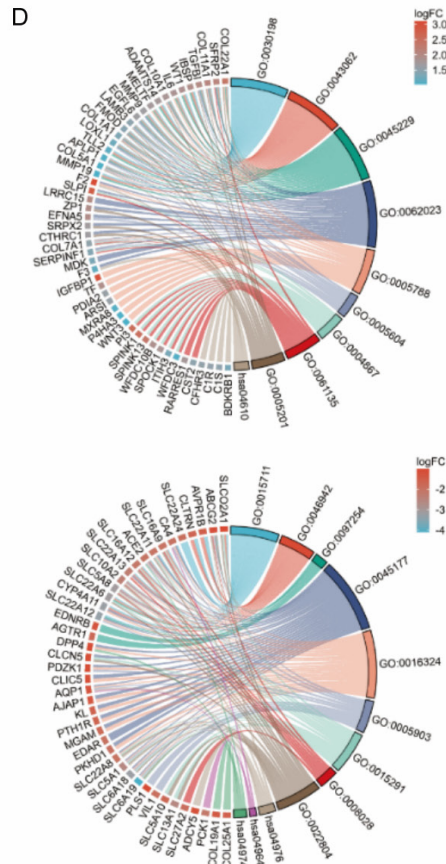
Figure 7. Prediction of downstream signaling pathways regulated by SAA2. A. Volcanic map displays differentially expressed genes grouped by SAA2 expression levels. B. Heat map of the top 10 differentially expressed genes upregulated and downregulated in the SAA2 high expression group. C. KEGG bar chart analysis shows possible signaling pathways downstream of SAA2. D. Chord plot analysis of potential genes downstream of SAA2 and their corresponding KEGG and GO pathways.

sion levels positively correlating with enhanced proliferative capacity and migratory potential. Functional interrogation revealed that shRNA-mediated SAA2 knockdown significantly suppressed RCC cell proliferation and migration, whereas ectopic SAA2 overexpression conversely amplified these oncogenic phenotypes.

All these functions collectively contribute to the tumor-promoting effects of SAA2 in various types of tumors. By integrating our findings with existing literature through comparative analysis, this study critically contextualizes the multifaceted role of SAA2 in tumorigenesis and malignant progression. For instance, studies have identified a correlation between SAA2 and tumorigenesis. Rogers et al. [25] found that 2-amino-1-methyl-6-phenylimidazo[4,5-b] pyridine (PhIP), a heterocyclic aromatic amine (HCA) ingested after meat is cooked at high temperatures, leads to an increase in transcription factors such as SAA2 through the JAK/STAT and MAPK pathways, thereby mediating the occurrence of cancer. Some studies have relied on serum concentrations of SAA2 to intervene in tumor patients at an earlier stage. Kim et al. [26] developed multiplexed parallel reaction monitoring (PRM) assays to analyze the isoforms of SAA proteins in plasma samples from lung cancer patients, aiming to facilitate early diagnosis and corresponding treatment for lung cancer patients. Similarly, Wu et al. [27] also evaluated the serum levels of SAA2 in differentiating gastric cancer from gastritis patients and developed a diagnostic model targeting the SAA family to distinguish gastritis from gastric cancer. Shi et al. [28] identified SAA2 as one of the driver genes for breast cancer metastasis through bioinformatics analysis. Xu et al. [29] found that SAA2 is associated with angiogenesis in pancreatic ductal adenocarcinoma. These studies, together with our findings, demonstrate that SAA2 plays a significant tumor-promoting role across multiple cancer types, though its specific mechanisms may vary depending on tumor type and microenvironment.

In RCC, we noticed that Cooley et al. [15] had previously generated multiple cell lines depicting the major stages of tumor progression through genomic analysis, and identified SAA2 as a soluble prognostic and predictive biomarker of therapeutic response through large-scale transcriptome, genome, and methylome analyses. Our current study also confirms this finding and validates the tumor-promoting role of SAA2 both in vitro and in vivo through specific experiments.

While this study primarily employed specific RCC cell lines and animal models, which are representative for investigating RCC pathogenesis, these models cannot fully recapitulate the extensive heterogeneity and clinical complexity of human renal cancer. For instance, tumor cells from different patients may exhibit diverse genetic mutations and biological behaviors, and the cell lines used in this study may not comprehensively reflect such interpatient variability, thereby partially limiting the generalizability of our findings. Although we experimentally validated the pro-tumorigenic role of SAA2 in both in vitro and in vivo settings, the exploration of its upstream regulatory mechanisms and downstream signaling pathways remains insufficiently comprehensive. Our current understanding of SAA2-mediated molecular networks in RCC progression relies predominantly on bioinformatic predictions rather than experimental validation. For example, while bioinformatic analyses predicted potential signaling pathways involving SAA2, the specific contributions and molecular mechanisms of these pathways in SAA2-driven RCC progression remain unverified experimentally, leaving gaps in our mechanistic comprehension.

Moreover, the nomogram prediction model developed in this study requires prospective validation with expanded cohorts to enhance its clinical applicability. Current limitations in sample size and single-center design necessitate multicenter validation to strengthen the evidence level and translational potential of this prognostic tool. Future studies should pri-

oritize functional validation of predicted pathways (e.g., CRISPR-based mechanistic dissection), incorporation of patient-derived organoid models to address tumor heterogeneity, and large-scale clinical validation to bridge these preclinical findings to therapeutic applications.

Conclusions

This study developed a prognostic nomogram model incorporating six genes (ZIC2, SAA2, ITPKA, SHOX2, TREML3P, and PDIA2) through bioinformatics analysis for predicting renal cell carcinoma outcomes. Furthermore, both in vitro and in vivo experiments validated that SAA2 promotes RCC proliferation and migration. We also predicted the downstream signaling pathways of SAA2, providing valuable insights for guiding clinical follow-up strategies.

Acknowledgements

Disclosure of conflict of interest

None.

Address correspondence to: Dr. Zhiyuan Zhuo, Department of Urology, Changhai Hospital, Naval Medical University, No. 168 Changhai Road, Shanghai 200433, China. E-mail: zhiyuanzhuo@qq.com

References

[1]   Sung H, Ferlay J, Siegel RL, Laversanne M, Soerjomataram I, Jemal A and Bray F. Global cancer statistics 2020: GLOBOCAN estimates of incidence and mortality worldwide for 36 cancers in 185 countries. CA Cancer J Clin 2021; 71: 209-249.

[2]   Hora M, Albiges L, Bedke J, Campi R, Capitanio U, Giles RH, Ljungberg B, Marconi L, Klatte T, Volpe A, Abu-Ghanem Y, Dabestani S, Fernandez-Pello S, Hofmann F, Kuusk T, Tahbaz R, Powles T, Bex A and Trpkov K. European Association of Urology Guidelines panel on renal cell carcinoma update on the New World Health Organization Classification of kidney tumours 2022: the urologist's point of view. Eur Urol 2023; 83: 97-100.

[3]   Rini BI, Campbell SC and Escudier B. Renal cell carcinoma. Lancet 2009; 373: 1119-1132.

[4]   Parmar A, Sander B, Bjarnason GA and Chan KKW. Systemic therapy in metastatic renal cell carcinoma: emerging challenges in therapeutic choice. Crit Rev Oncol Hematol 2020; 152: 102971.

[5]   Dudani S, Savard MF and Heng DYC. An update on predictive biomarkers in metastatic renal cell carcinoma. Eur Urol Focus 2020; 6: 34-36.

[6]   Young M, Jackson-Spence F, Beltran L, Day E, Suarez C, Bex A, Powles T and Szabados B. Renal cell carcinoma. Lancet 2024; 404: 476-491.

[7]   Pecoraro A, Palumbo C, Knipper S, Mistretta FA, Rosiello G, Tian Z, St-Hilaire PA, Shariat SF, Saad F, Lavallee L, Briganti A, Kapoor A, Fiori C, Porpiglia F and Karakiewicz PI. Synchronous metastasis rates in T1 renal cell carcinoma: a surveillance, epidemiology, and end results database-based study. Eur Urol Focus 2021; 7: 818-826.

[8]   Choueiri TK and Motzer RJ. Systemic therapy for metastatic renal-cell carcinoma. N Engl J Med 2017; 376: 354-366.

[9]   Ivanyi P, Frohlich T, Grunwald V, Zschabitz S, Bedke J and Doehn C. The treatment of metastatic renal cell carcinoma. Dtsch Arztebl Int 2024; 121: 576-586.

[10]   Elinav E, Nowarski R, Thaiss CA, Hu B, Jin C and Flavell RA. Inflammation-induced cancer: crosstalk between tumours, immune cells and microorganisms. Nat Rev Cancer 2013; 13: 759-771.

[11]   Coussens LM and Werb Z. Inflammation and cancer. Nature 2002; 420: 860-867.

[12]   Diakos CI, Charles KA, McMillan DC and Clarke SJ. Cancer-related inflammation and treatment effectiveness. Lancet Oncol 2014; 15: e493-503.

[13]   Sack GH Jr. Serum amyloid A - a review. Mol Med 2018; 24: 46.

[14]   Malle E and De Beer FC. Human serum amyloid A (SAA) protein: a prominent acute-phase reactant for clinical practice. Eur J Clin Invest 1996; 26: 427-435.

[15]   Cooley LS, Rudewicz J, Souleyreau W, Emanuelli A, Alvarez-Arenas A, Clarke K, Falciani F, Dufies M, Lambrechts D, Modave E, Chalopin-Fillot D, Pineau R, Ambrosetti D, Bernhard JC, Ravaud A, Negrier S, Ferrero JM, Pages G, Benzekry S, Nikolski M and Bikfalvi A. Experimental and computational modeling for signature and biomarker discovery of renal cell carcinoma progression. Mol Cancer 2021; 20: 136.

[16]   Lee JY, Hall JA, Kroehling L, Wu L, Najar T, Nguyen HH, Lin WY, Yeung ST, Silva HM, Li D, Hine A, Loke P, Hudesman D, Martin JC, Kenigsberg E, Merad M, Khanna KM and Littman DR. Serum amyloid a proteins induce pathogenic Th17 cells and promote inflammatory disease. Cell 2020; 180: 79-91, e16.

[17] Bang YJ, Hu Z, Li Y, Gattu S, Ruhn KA, Raj P, Herz J and Hooper LV. Serum amyloid A delivers retinol to intestinal myeloid cells to promote adaptive immunity. Science 2021; 373: eabf9232.

[18] Gao X, Sun R, Jiao N, Liang X, Li G, Gao H, Wu X, Yang M, Chen C, Sun X, Chen L, Wu W, Cong Y, Zhu R, Guo T and Liu Z. Integrative multiomics deciphers the spatial characteristics of host-gut microbiota interactions in Crohn's disease. Cell Rep Med 2023; 4: 101050.

[19] Liu Y, Liu J, Liu A, Yin H, Burd I and Lei J. Maternal siRNA silencing of placental SAA2 mitigates preterm birth following intrauterine inflammation. Front Immunol 2022; 13: 902096.

[20] Olivier DW, Eksteen C, Plessis MD, de Jager L, Engelbrecht L, McGregor NW, Shridas P, de Beer FC, de Villiers WJS, Pretorius E and Engelbrecht AM. Inflammation and tumor progression: the differential impact of SAA in breast cancer models. Biology (Basel) 2024; 13: 654.

[21] Yamamoto K, Shiroo M and Migita S. Diverse gene expression for isotypes of murine serum amyloid A protein during acute phase reaction. Science 1986; 232: 227-229.

[22] Stone ML, Lee J, Lee JW, Coho H, Tariveranmoshabad M, Wattenberg MM, Choi H, Herrera VM, Xue Y, Choi-Bose S, Zingone SK, Patel D, Markowitz K, Delman D, Balachandran VP and Beatty GL. Hepatocytes coordinate immune evasion in cancer via release of serum amyloid A proteins. Nat Immunol 2024; 25: 755-763.

[23] Meek RL, Hoffman JS and Benditt EP. Amyloidogenesis. One serum amyloid A isotype is selectively removed from the circulation. J Exp Med 1986; 163: 499-510.

[24] Kluve-Beckerman B, Dwulet FE and Benson MD. Human serum amyloid A. Three hepatic mRNAs and the corresponding proteins in one person. J Clin Invest 1988; 82: 1670-1675.

[25] Rogers LJ, Basnakian AG, Orloff MS, Ning B, Yao-Borengasser A, Raj V and Kadlubar S. 2-amino-1-methyl-6-phenylimidazo(4,5-b) pyridine (PhIP) induces gene expression changes in JAK/STAT and MAPK pathways related to inflammation, diabetes and cancer. Nutr Metab (Lond) 2016; 13: 54.

[26] Kim YJ, Gallien S, El-Khoury V, Goswami P, Sertamo K, Schlesser M, Berchem G and Domon B. Quantification of SAA1 and SAA2 in lung cancer plasma using the isotype-specific PRM assays. Proteomics 2015; 15: 3116-3125.

[27] Wu DC, Wang KY, Wang SSW, Huang CM, Lee YW, Chen MI, Chuang SA, Chen SH, Lu YW, Lin CC, Lee KW, Hsu WH, Wu KP and Chen YJ. Exploring the expression bar code of SAA variants for gastric cancer detection. Proteomics 2017; 17.

[28] Shi Y, Zhang D, Chen J, Jiang Q, Song S, Mi Y, Wang T and Ye Q. Interaction between BEND5 and RBPJ suppresses breast cancer growth and metastasis via inhibiting Notch signaling. Int J Biol Sci 2022; 18: 4233-4244.

[29] Xu H, Hua J, Meng Q, Wang X, Xu J, Wang W, Zhang B, Liu J, Liang C, Yu X and Shi S. Hyperdense pancreatic ductal adenocarcinoma: clinical characteristics and proteomic landscape. Front Oncol 2021; 11: 640820.